Occurrence and cycling of dimethylated sulfur compounds in the Arctic during summer receding of the ice edge

Martí Galí [*], Rafel Simó

Department of Marine Biology and Oceanography, Institut de Ciències del Mar (CSIC), Pg. Marítim de la Barceloneta 37-49, 08003 Barcelona, Catalonia, Spain

ABSTRACT

The distribution and cycling of dimethylsulfide (DMS), dimethylsulfoniopropionate (DMSP) and dimethyl-sulfoxide (DMSO) were studied in the Greenland Sea and Arctic Ocean during July 2007. The concentration of these compounds was analyzed in vertical profiles of the top 100 m of the water column, with special emphasis on the subsurface (1 m) and the immediate subsurface waters (0.1 m). Seawater incubations were conducted in order to measure the rates of biological DMS cycling, as well as DMS photolysis rates. DMS ventilation rates were calculated from the hourly meteorological time series. Moderate concentrations of DMS (0.1 to 18.3 nM), DMSP (1.4 to 163.6 nM) and DMSO (9.0 to 84.7 nM) were found, considering that elevated biomasses of the haptophyte *Phaeocystis pouchetii* dominated in the study area. The overall situation was characterized by a tight coupling of biological DMS production and consumption, and a fast biological turnover of DMS (0.5 to 4 days). Bacterial consumption was the dominant sink for DMS, accounting for 9–73% of its loss in the upper mixed layer (UML). However, the shallow stratification encountered (mixed layer depth between 1.5 and 11 m) enhanced DMS photolysis, which accounted for 12–65% of the total DMS loss and, at some stations, became the dominant sink. DMS production followed phytoplankton biomass (and DMSP concentration) in surface waters, while bacterial DMS consumption was controlled by the depth of the UML (presumably through exposure to solar radiation). Ice melt drove surface stratification, regulating the entrainment of cells and materials into the upper layer from the more productive waters below, and eventually the fraction of DMS escaping to the atmosphere.

© 2010 Elsevier B.V. All rights reserved.

1. Introduction

Dimethylsulfide (DMS) is the most abundant volatile sulfur compound in the surface ocean, and represents the major natural source of reduced sulfur to the global troposphere (Andreae and Crutzen, 1997). DMS is mainly produced by the enzymatic cleavage of its biological precursor dimethylsulfoniopropionate (DMSP), an abundant and widespread intracellular compound found in marine microalgae (Keller et al., 1989) and in other halophytic plants.

Research on DMS was first stimulated by the realization that this gas could account for the "missing" flux of sulfur from the oceans to the atmosphere that closes the budget of this essential element at the global scale (Lovelock et al., 1972), and was further encouraged when its involvement in a climatic regulatory feedback was proposed (Charlson et al., 1987). The latter authors hypothesized that the oxidation of DMS in the atmosphere would modify the albedo of clouds through the development of cloud condensation nuclei, thus altering the radiative budget over the oceans. If, in turn, DMS production by the marine microbiota was dependent on sea surface irradiance or temperature, the loop would be closed, establishing a negative plankton–climate feedback.

Since this hypothesis was postulated, our knowledge of the marine cycle of DMS and DMSP has rapidly increased, either from the physiological, ecological or the biogeochemical point of view. Several physiological functions have been proposed for DMSP: osmoregulator and cryoprotectant (Malin and Kirst, 1997; Welsh, 2000), methyl donor in metabolic reactions (Kiene et al., 1999), overflow mechanism for excess reducing power under conditions of unbalanced growth (Stefels, 2000), and the initial compound in a cascade of oxidations (involving its breakdown products DMS, acrylate, dimethylsulfoxide (DMSO) and methane sulfinic acid) that would prevent oxidative stress in cells (Sunda et al., 2002). Moreover, DMSP plays a critical role in marine microbial food webs, both as a chemical signal (Wolfe, 2000; Zimmer-Faust et al., 1996), and as the main carrier of reduced S and a significant carrier of C within and among trophic levels (Kiene et al., 2000; Simó et al., 2002).

DMSP production by phytoplankton displays a large variability, both across taxonomic groups (Keller et al., 1989) and within taxa depending on environmental conditions (Stefels et al., 2007). The cleavage of DMSP to DMS can proceed through different enzymatic pathways in the microbial food web, generally referred to as 'DMSP lyases'. These are found in some algal and bacterial taxa, and can be

* Corresponding author.
E-mail address: mgali@icm.csic.es (M. Galí).

intra- or extracellular (Stefels and Dijkhuizen, 1996; Yoch et al., 1997). DMSP release to the dissolved phase, eventually promoting DMS production, takes place upon grazing, viral lysis and phytoplankton autolysis (Simó, 2001). However, a competing, non DMS-producing pathway for DMSP degradation ubiquitously exists, by which bacteria demethylate DMSP and eventually assimilate its sulfur (Kiene et al., 2000; Howard et al., 2006). The widespread uptake of DMSP by marine phytoplankton (Vila-Costa et al., 2006b) further complicates the picture.

Once in seawater, DMS has three dominant fates: ventilation to the atmosphere, photooxidation, and microbial (bacterial) consumption, which usually represents its major sink (Simó, 2004). In the latter two processes dissolved dimethylsulfoxide (DMSO) is one of the products (del Valle et al., 2007a; Kieber et al., 1996). Phytoplankton can also produce and release DMSO (Simó et al., 1998), but its possible physiological roles remain uncertain, although functions similar to those of DMSP have been proposed (Lee and de Mora, 1999; Sunda et al., 2002). In summary, DMSO is a major pool of organic sulfur in the ocean (Hatton et al., 2004; Simó and Vila-Costa, 2006), and its pivotal role in dimethylated sulfur cycling is progressively being unveiled.

Due to the complexity and number of interactions explained above, fully mechanistic models often fail to predict seawater DMS concentrations (Simó and Dachs, 2002). Comprehensive field studies, therefore, are of great importance as they provide further gains in understanding as well as the grounds against which hypotheses, laboratory results and model outputs can be validated. In the context of climate change, studies on the biogeochemical functioning and air–sea interactions of marine ecosystems already undergoing visible changes are very relevant, especially if existing data for the area under study are relatively scarce. The Arctic Ocean is predicted to be among the areas most affected by the ongoing climate change (IPCC, 2007; Johannessen et al., 2004; Moritz et al., 2002). In addition, in the late summer of 2007 the lowest ice extent was observed since the start of satellite records in 1979 (Stroeve et al., 2008). The aim of our study is to provide a better understanding of the distribution and cycling of dimethylated sulfur compounds in open-ocean and ice-margin waters during the Arctic ice melt, and the processes controlling the fraction of biologically produced DMS that ends up in the atmosphere.

2. Methods

2.1. Sample collection and CTD profiles

During the ATOS1 Arctic cruise, carried out in July 2007, a total of 49 stations were occupied, of which 17 were sampled for dimethylated sulfur compounds. Deck board incubation experiments were conducted in 8 of these. Most stations were located NW of the Svalbard archipelago, between 80° N–81° N and 5°E–20° E, except for the initial stations that covered the transect from the north of Iceland to NW Svalbard, across the East Greenland Current (EGC) and the Fram Strait.

Samples for DMS(P,O) profiles were collected every morning at 8 am from 5 depths in the top 200 m of the water column, using Niskin bottles attached to a CTD rosette (Seabird SBE 911). Silicone tubing was used to fill 120 ml glass vials to the top (without head space), allowing some overflow and taking care to avoid bubbling. An additional Niskin bottle was deployed to sample at 1 m depth. At some stations, an extra sample from 0.1 m depth was taken from a Zodiac inflatable boat by pumping seawater through acid-cleaned Teflon tubing to a 0.25 L Teflon bottle. All bottles were cleaned with hydrochloric acid before the cruise started, and from then on they were rinsed several times with MQ water after each use, and with sample seawater before they were filled.

At 4 stations in the Fram Strait area, DMSP and DMSO were also analyzed in sea ice samples obtained with a coring device (Mark III, Kovacs Enterprise Inc.). Only the top and bottom 20 cm of the ice cores (which were 1 m long and 7.25 cm in diameter) were used after melting overnight in acid-washed Teflon (PFA) bags at room temperature. The ice melt water was sampled with a syringe from the Teflon bags and analyzed like seawater samples.

In addition to temperature, conductivity (salinity) and pressure (depth), the variables measured in CTD profiles included fluorescence of chlorophyll *a,* beam attenuation (c_p) at 660 nm (a proxy for total biogenic particle mass, i.e. particulate organic carbon) and turbidity. Vertical profiles were binned and averaged in 1 m intervals. Density (sigma-t) was calculated from temperature and salinity with the built-in algorithm of the *Ocean Data View* software (Schlitzer, 2008). The mixed layer depth (MLD) was defined as the maximum depth before a step in density bigger than 0.02 kg m^{-4} was encountered. At all stations (except Stn. 1), shipborne CTD profiles of the uppermost water column were checked against the more reliable temperature and salinity profiles obtained from the zodiac boat, which covered the 3 upper meters of the water column.

Both fluorescence and extracted Chl *a* are poor indicators of algal biomass, for they are affected by photoadaptation and nutrient stress (Behrenfeld and Boss, 2003). Consequently, we chose beam attenuation (c_p) as our reference variable for planktonic microbial biomass. Even though c_p also accounts for heterotrophic bacterial biomass (Oubelkheir et al., 2005), the proportion of autotrophic biomass is expected to increase as we move towards eutrophic conditions (Gasol et al., 1997) and will probably dominate during strong phytoplankton bloom conditions.

2.2. Analysis of sulfur compounds

Dimethylated sulfur compounds were analyzed by purging, cryotrapping and sulfur-specific gas chromatography followed by flame photometry (Simó et al., 1996). The detection limit was ca. 3 pmol S. To analyze DMS, 3-5 ml of seawater were gently filtered through a GF/F syringe filter and immediately sparged in a crimp glass vial. A larger volume of sample (40 ml) was stored in crimp glass vials, where two pellets (45 mg each) of NaOH were added. DMS was analyzed within 1 h after collection. Total DMSP (DMSPt) was analyzed the following day, except for a few samples that were run on land within 2 months after the cruise had finished. Total DMSO (DMSOt) was analyzed within a few months in the same vials, after purging with N_2 the DMS evolved from alkaline DMSP cleavage. DMSO was measured as DMS after reduction by $NaBH_4$, added in its cobalt-doped form to skip the neutralization step (Simó and Vila-Costa, 2006). All samples were analyzed in duplicate, and the median coefficient of variation between replicates was 5.2, 6.3 and 3.5% for DMS, DMSPt and DMSOt respectively.

The attempts made to measure dissolved DMSP (DMSPd) by the small-volume gravity drip filtration method (Kiene and Slezak, 2006) repeatedly failed, due to the presence of the colony-forming haptophyte *Phaeocystis.* The colonies and even the solitary cells of this small flagellate easily break down upon filtration, releasing the intracellular content (Schoemann et al., 2005). For this same reason, a prefiltering step through a 50 μm mesh was carefully applied when filling the vials destined for DMS analysis. This step prevents artifacts in the measurement of DMS, caused by the elevated concentrations of DMSP and DMSP lyases in solution.

2.3. Biological process incubations

For the determination of gross DMS production by the whole microbial community and bacterial DMS consumption, water from 1 m depth and from the depth of the fluorescence maximum was incubated in the dark at the in situ surface temperature ± 1 °C. For that purpose, amber glass bottles (2.9 L) were directly filled from the Niskin bottles. One unamended bottle was incubated as a control, along with a second bottle that was amended with ca. 250 nM of

dimethyldisulfide (DMDS), an effective inhibitor of bacterial DMS consumption (Wolfe and Kiene, 1993; Simó et al., 2000). The duration of the incubations was around 20 h, during which the inhibitory effect generally held. Otherwise, only the part of the incubation with a linear DMS accumulation was used for the calculations. The slope of the linear regression between DMS concentration and incubation time in the control bottles provided the net DMS production rate. The slope of the DMDS amended treatment yielded the rate of the community gross DMS production. The bacterial DMS consumption rate was obtained as the difference between gross and net DMS production rates. DMSPt was also monitored in the control incubations. At Stn. 42, surface seawater was also incubated in the light under the same irradiance as the photochemistry incubations using 2.3 L Teflon bottles (see *Results, Dark versus light incubation*).

2.4. DMS photolysis

2.4.1. Incubation setup

DMS photolysis rates were measured at stations 20, 26, 39 and 42 in either 75 ml quartz flasks or 250 ml Teflon bottles (Stn. 42) incubated on board. Seawater from 1 m depth was gravity filtered through GF/F, and then syringe filtered through 0.2 µm Nylon membranes. DMS was added to concentrations of 20–70 nM in order to ensure that photooxidation of DMS was detectable within incubation times, and the water was transferred to the bottles leaving no head space. Duplicate light and dark bottles (the latter wrapped in aluminum foil) were kept for 7–12 h in a bath with running seawater from the ship's underway intake, while solar radiation and bath temperature were recorded continuously. The incubation tank was covered with a neutral screen that attenuated 52% of the solar radiation in the ultraviolet (UV) and in the photosynthetically active radiation (PAR) regions.

2.4.2. Rate constant calculation

The photolysis rate constant (K_{photo}, d^{-1}) was calculated assuming a pseudo first-order kinetics (Brimblecombe and Shooter, 1986; Kieber et al., 1996; Brugger et al., 1998; Hatton, 2002). Concentrations from duplicate bottles were averaged, and final concentrations in the light were corrected for any changes happened in the dark. The natural logarithms of initial and final DMS concentrations were plotted against time after dark correction, and the slope was taken as the K_{photo}. A correction factor was applied at Stn. 42 to account for the slightly lower transmittance of Teflon bottles in the UV range compared to quartz.

2.4.3. CDOM measurements

Absorption spectra of chromophoric dissolved organic matter (CDOM) were measured in the GF/F filtrates used for DMS photolysis before and after the incubations. Spectrophotometric scans (280 to 800 nm) were performed in a 1 cm pathlength (r) quartz cuvette, and spectral absorption coefficients were calculated from spectral absorbance ($A_{CDOM,\lambda}$) after subtracting the absorbance of MQ water, as $a_{CDOM,\lambda} = 2.303\ A_{CDOM,\lambda} \cdot r^{-1}$. Analysis of 0.2 µm filtrates showed minor differences with GF/F filtrates. The spectral slope of CDOM ($S_{300-400}$) was computed from the linear regression between the natural logarithm of $a_{CDOM,\lambda}$ and wavelength, in the range of 300–400 nm. In some samples, marked absorption peaks occurred around 330 nm, which were attributed to mycosporine-like aminoacids. In those occasions, the peaks were excluded from the linear regression.

2.5. Upper mixed layer-averaged solar radiation and optical calculations

2.5.1. Attenuation coefficients (K_d) and UML-averaged solar radiation

Diffuse attenuation coefficients for downward radiation (K_d) were calculated as the slope of the linear regression between the natural logarithm of downwelling irradiance and depth: $ln(E_{d,z,\lambda}) = K_{d,\ \lambda} \cdot z$.

Only the UML, or alternatively, a deeper and optically homogeneous surface layer, were used for K_d calculation, so that the r^2 of the regression was above 0.98 at all stations considered. The minutely time series from the ship's meteorological station was used to calculate the mean irradiance during the 24 h prior to sample collection. This value was converted to subsurface irradiance ($E_{d,o-}$) with a 10% surface reflectance applied, based on mean wind speed and solar zenith angle (Kirk, 1994), and then the average depth-integrated solar radiation in the UML was calculated (following Vallina and Simó, 2007): $E_{d,UML} = (E_{d,o-} / (K_{d,PAR} \cdot MLD)) \cdot (1 - exp(K_{d,PAR} \cdot MLD))$.

2.5.2. Averaged spectral irradiance in photolysis experiments

A PAR–UV radiometer (Biospherical PUV 2500) was placed in the center of the incubation tank to keep a continuous record of the solar radiation reaching the samples. Downwelling cosine irradiance was measured at a frequency of 5 s^{-1} in six bands in the UV region (centered at 305, 313, 320, 340, 380 and 395 nm) and one integrated band in the visible region (PAR). The mean spectral irradiance during the incubation was obtained for each UV band, and the total energy received in the UVB and UVA was computed as the integral of mean spectral irradiance over a given spectral interval and time.

The time series from the meteorological station of the ship was used to calculate the time-integrated total irradiance reaching the samples after successively crossing the neutral screen (52% attenuation) and the water surface (10% reflectance). The K_{photo} obtained in bottle experiments were converted to in situ mixed layer photolysis rate constants ($K_{photo,UML}$) according to the following steps: first, a subsurface in situ rate constant was obtained as the product of the experimental K_{photo} by the average in situ subsurface irradiance divided by the averaged incubation irradiance; second, a depth-averaged $K_{photo,UML}$ was calculated in the same manner as $E_{d,UML}$, but assuming that K_{photo} decayed exponentially with the K_d of 340 nm radiation. Our calculations indicated that 340 nm was the wavelength at which maximum DMS photolysis occurred in surface waters, according to the product of light absorption (CDOM spectra) by the apparent quantum yield of DMS photolysis obtained by Deal et al. (2005) in the Bering Sea.

2.6. Sea–air DMS flux

Hourly DMS fluxes were calculated using the subsurface DMS concentration (1 m depth, and 0.1 m depth when available) and the hourly wind speeds from the ship's meteorological station, and were then averaged on a daily basis. The parameterization of Nightingale et al. (2000) was used to obtain $k_{w,DMS}$, the transfer or piston velocity of DMS (cm h^{-1}): $k_{w,DMS} = ((5.88\ u_{10}^2) + (1.49\ u_{10})) \cdot Sc^{-1/2}$, where u_{10} = wind speed at 10 m height (m s^{-1}); Sc = Schmidt number of DMS, calculated from the sea surface temperature according to Saltzman et al. (1993). Emission fluxes (F_{DMS}) were then obtained as the product of DMS in seawater (C_w, which drives the flux) and the transfer velocity: $F_{DMS} = 0.24\ k_{w,DMS} \cdot C_w$. Finally, ventilation rate constants in the UML ($K_{vent,UML}$) were obtained as the surface flux divided by DMS concentration and MLD.

2.7. Statistical analysis

2.7.1. Grouping of stations

Vertical profiles of CTD variables were used to construct a classification of the 17 stations where sulfur data were available. Briefly, profiles of each variable between 0 and 30 m were grouped using cluster analysis (cityblock, cutoff = 1). The resulting groups had characteristic depth profiles of the selected variable. This rendered as many different classifications as variables used. However, salinity and c_p showed a strong agreement, and were therefore used as the defining criteria (see *Results*). The average profiles ($\pm$ SE) of representative CTD variables were calculated for each group.

2.7.2. Vertical profiles

A correlation matrix (Pearson correlation) allowed the exploration of the relationships between sulfur compounds and biotic and abiotic parameters measured from CTD casts. In addition, stepwise regression was performed in order to find the most significant predictors for DMS, DMSPt and DMSOt. Stepwise regression was judged a convenient technique to prevent collinearity artifacts in the multiple regression, that is, artifacts caused by highly correlated variables within the predictor matrix. The initial model included no terms, and the entrance tolerance for additional terms was $p < 0.05$.

2.7.3. Surface distribution and biological cycling

Surface distribution of dimethylated sulfur compounds, planktonic biomass and related abiotic parameters, and biological sulfur cycling were explored by means of correlation analysis. Given the low number of data points available (<20), the non-parametric Spearman correlation method was used.

3. Results

3.1. Oceanographic setting

3.1.1. Physical features

The transect from Iceland to the north of Svalbard archipelago is characterized by the interaction between warm and salty Atlantic Water (AW), which flows northwards forming the West Svalbard Current (WSC), and the southwards overflow of Arctic Water through the Fram Strait (between Svalbard and Greenland) and along the Greenland shelf, forming the East Greenland Current (EGC; Rudels et al., 2005; Fig. 1A, B). In the Fram Strait and on the Yermak Plateau (NW of Svalbard) mixing between these water masses occurs, and recirculated AW is entrained
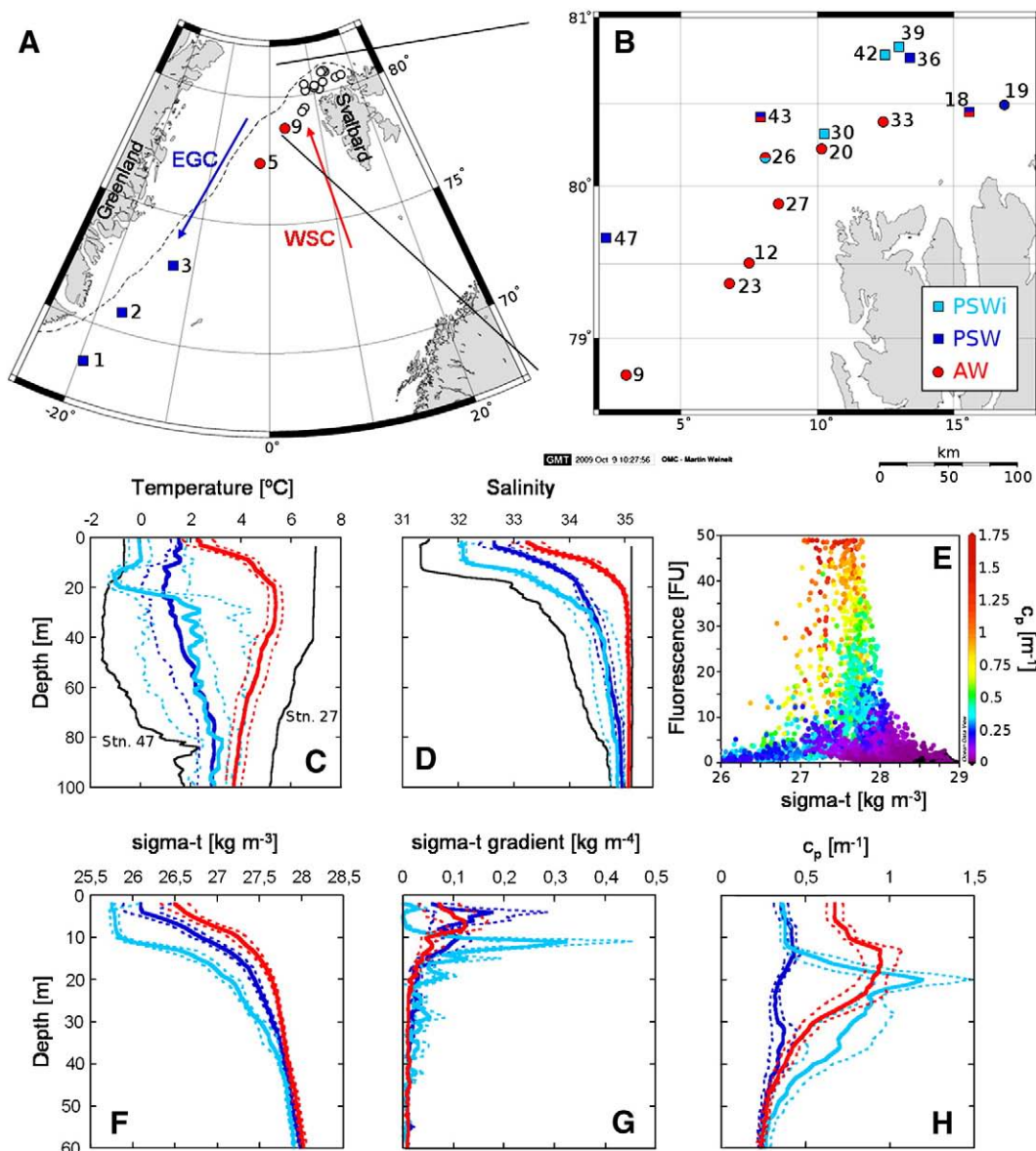
Fig. 1. Map of the stations where sulfur measurements were performed and synthesis of the oceanographic setting. A) whole study area and main currents: EGC (East Greenland Current) and WSC (West Svalbard Current) with the approximate location of the sea ice edge (dashed line); B) closer look to the Fram Strait Area. Note that non-sampled Stns. 27 and 47 are added as references of water mass end members. Red circles denote AW, dark blue squares PSW and light blue squares denote PSWi. Symbols in two colors represent those stations where classifications based on salinity (upper) and c_p (lower) disagreed; C) temperature and D) salinity, with the end member stations in black; E) diagram showing the occurrence of the deep fluorescence maximum on a well constrained isopycnal surface, and the complementary information given by c_p.; F) density, G) density gradient and H) c_p for the aforementioned three groups. Vertical profiles are average ± SE. (For interpretation of the references to colour in this figure legend, the reader is referred to the web version of this article.)

Table 1

Main characteristics of stations occupied during the cruise. Only Stns. 18 and 19 were on the continental shelf. Water masses are defined as Atlantic Water (AW, West Svalbard Current), Polar Surface Water (PSW) and PSW with highest or more recent ice influence (PSWi). Temperature, salinity, sigma-t and c_p are UML averages, practically equivalent to surface values. Irradiance and wind speed are the average for the 24 h prior to sampling. The asterisk (*) denotes stations where sea ice was close to the ship during sampling (up to 60% ice cover). Sulfur data available: Is = surface water (1 m) incubation; Id = fluorescence maximum incubation; p = complete profile; (p) = profile with less than 6 depths; photo = photochemistry; and surface = surface DMS, DMSPt and DMSOt measured.

Station	Date (2007)	Latitude (N)	Longitude (E)	Water mass	T ML (°C)	Sal ML	Sigma-t (kg m^{-3})	MLD (m^{-1})	$K_{d,PAR}$ (m^{-1})	c_p (m^{-1})	Irradiance (W m^{-2})	Wind speed (m s^{-1})	Sulfur data available
1	7/1	68 28.81	− 19 30.30	PSW	2.4	32.7	25.9	6	0.11	0.36	NA	NA	Is, Id, p
2	7/2	70 43.26	− 17 08.17	PSW	2.0	31.7	25.3	2	0.11	0.28	118	4.9	p
3	7/3	72 57.23	− 12 39.67	PSW	2.3	31.8	25.4	2	0.11	0.33	113	3.0	Is, Id, p
5	7/5	77 23.23	− 1 39.82	AW	2.7	33.8	26.9	6	0.29	0.90	134	4.3	(p)
9	7/7	78 43.72	2 58.49	AW*	2.6	33.7	26.9	5	0.24	0.78	210	7.8	Is, Id, (p)
12	7/8	79 30.80	7 29.64	AW*	1.4	32.8	26.2	3	0.20	0.57	145	5.7	Is, Id, p
18	7/10	80 26.96	13 37.59	PSW	1.6	33.3	26.5	11	0.11	0.79	274	10.3	surface
19	7/11	80 29.28	16 53.28	PSW*	1.5	33.6	26.9	7	NA	0.62	147	3.7	Is
20	7/12	80 13.99	10 11.44	AW*	0.1	32.3	25.9	5	0.17	0.52	222	3.3	Is, Id, p, photo
23	7/13	79 22.18	6 49.54	AW	5.3	34.3	27.1	7	0.21	0.61	268	5.6	surface
26	7/14	80 09.93	8 05.16	AW*	1.6	32.3	25.8	1.5	0.13	0.41	238	4.6	Is, (p), photo
30	7/16	80 19.12	10 17.70	PSWi*	0.5	32.2	25.8	9	0.13	0.36	360	7.1	surface
33	7/17	80 23.61	12 26.15	AW*	2.0	33.2	26.5	6	0.13	0.52	242	5.9	surface
36	7/18	80 46.47	13 21.11	PSW*	0.0	31.9	25.6	2	0.11	0.31	159	6.4	surface
39	7/19	80 49.57	13 14.22	PSWi*	0.3	32.0	25.7	9	0.11	0.36	82	7.8	Is, p, photo
42	7/20	80 47.16	12 32.04	PSWi*	-0.9	32.1	25.8	10	0.13	0.38	93	8.0	Is, photo
43	7/21	80 22.72	7 52.70	PSW	0.7	33.2	26.6	11	0.18	0.68	99	8.4	surface

into the EGC which, further south, progressively loses the low temperature and salinity characteristic of Polar Surface Water (PSW). In our cruise, the AW end member showed a temperature maximum of ca. 7 °C in the UML, while PSW had a temperature minimum of almost −1.8 °C at around 40 m depth (Fig. 1C). Sea surface temperature ranged from −1 to 7 °C. Salinity usually decreased from a value of 35 at 100 m to reach values between 31 and 35 at surface (Fig. 1D).

3.1.2. Classification of the stations

According to vertical profiles of salinity and its grouping with cluster analysis (see *Methods*), stations were divided in AW and PSW (Fig. 1, Table 1). Additionally, the latter group included a subgroup of stations that showed a stronger influence of ice melt, which will be referred to as PSWi. These groups showed distinct vertical profiles of physical variables, but also a distinct pattern of biomass distribution with depth. The cluster based on c_p profiles was highly consistent with that based on salinity, with only 3 out of 17 stations misclassified. This means that, despite the spatial variability induced by ice melt and mixing between water masses, there was a consistency between the physical setting and the timing and extent of the phytoplankton bloom. Schematically, it can be said that the bloom was triggered by ice melt-induced stratification of nutrient-rich AW as it moved northwards. The progressive input of meltwater pushed down the biomass maximum, which occurred deepest at those stations most influenced by ice (PSWi). Finally, the bloom progressively declined as nutrient-exhausted waters were recirculated south by the EGC.

3.1.3. Biological features

Elevated productivity and biomass were widespread features throughout the cruise. Compared to vertical profiles of either fluorescence or Chl *a*, c_p profiles did not display such a sharp decrease in biomass towards the surface (Fig. 1E). Biomass at the c_p maximum was around 1 m^{-1} in AW and PSWi stations, which approximately corresponded to a chlorophyll *a* concentration of 4 µg L^{-1}. Biomass in the UML was lower at PSW and PSWi stations (<0.5 m^{-1}, chlorophyll <1 µg L^{-1}) while it remained high (>0.5 m^{-1}, chlorophyll >1 µg L^{-1}) at those stations less influenced by ice (AW). These values are rather typical of the transition between bloom and post-bloom conditions in this area and time of the year (Sakshaug, 2004). Phytoplankton biomass was generally dominated by the haptophyte *Phaeocystis pouchetii*, although dinoflagellates, diatoms and other nanoflagellates made significant contributions at some stations (Calbet et al., submitted for

publication). A highest proportion of heterotrophic biomass was found at EGC stations, supporting our view of the temporal–spatial progression of the bloom. *P. pouchetii* , like its close relatives *P. globosa* and *P. antarctica*, is known for its ability to form quasi-monospecific blooms, and for the production of a mucilaginous polysaccharide matrix in which cells are embedded, forming large colonies (Schoemann et al., 2005). A relevant feature of bloom-forming *Phaeocystis* species is their elevated intracellular DMSP concentration (generally well above 100 mM) and DMSP lyase activity (Stefels and Van Boekel, 1993; Stefels and Dijkhuizen, 1996), which can give rise to elevated concentrations of DMS and acrylate in seawater.

3.1.4. Radiation climate in the UML

As a result of ice thaw (together with light winds) a strong and shallow stratification of the surface water column was found during our cruise: the MLD ranged from 1.5 to 11 m (mean of 6 m). Due to the vertical distribution of microorganisms, the UML was more transparent than the waters beneath. The vertical diffuse attenuation coefficient for downwelling PAR (K_d) was on average 0.15 m^{-1} (with values spanning between 0.11–0.29 m^{-1}). Light extinction in the UML was governed by biogenic materials, as demonstrated by the positive correlation between K_d and c_p ($r^2 = 0.59$, p<0.001, n = 17). Consequently, the differences in surface biomass translated into different PAR and UV transparencies between AW and PSW(i) (Table 1). Overcast and misty skies predominated in the beginning and the end of the cruise, so that a low mean surface irradiance of 180 W m^{-2} was recorded (total solar spectrum). However, the combination of very shallow and moderately clear mixed layers with 24 h of continuous sunlight rendered notable daily UML-averaged irradiances (mean 119, range 43–217 W m^{-2}). These values fall in the mid-upper range of values found in the world oceans (Vallina and Simó, 2007). According to the calculated vertical attenuation coefficients for downward irradiance, the UML was exposed, on average, to >10% and >1% of subsurface UVA and UVB radiation (respectively) in most stations.

3.2. Dimethylated sulfur concentrations

3.2.1. Vertical profiles

DMSPt concentrations in the study area closely followed phytoplankton biomass, generally peaking at the c_p maximum (Fig. 2, and see Matrai et al., 2007). In the upper 40 m of the water column (roughly, the
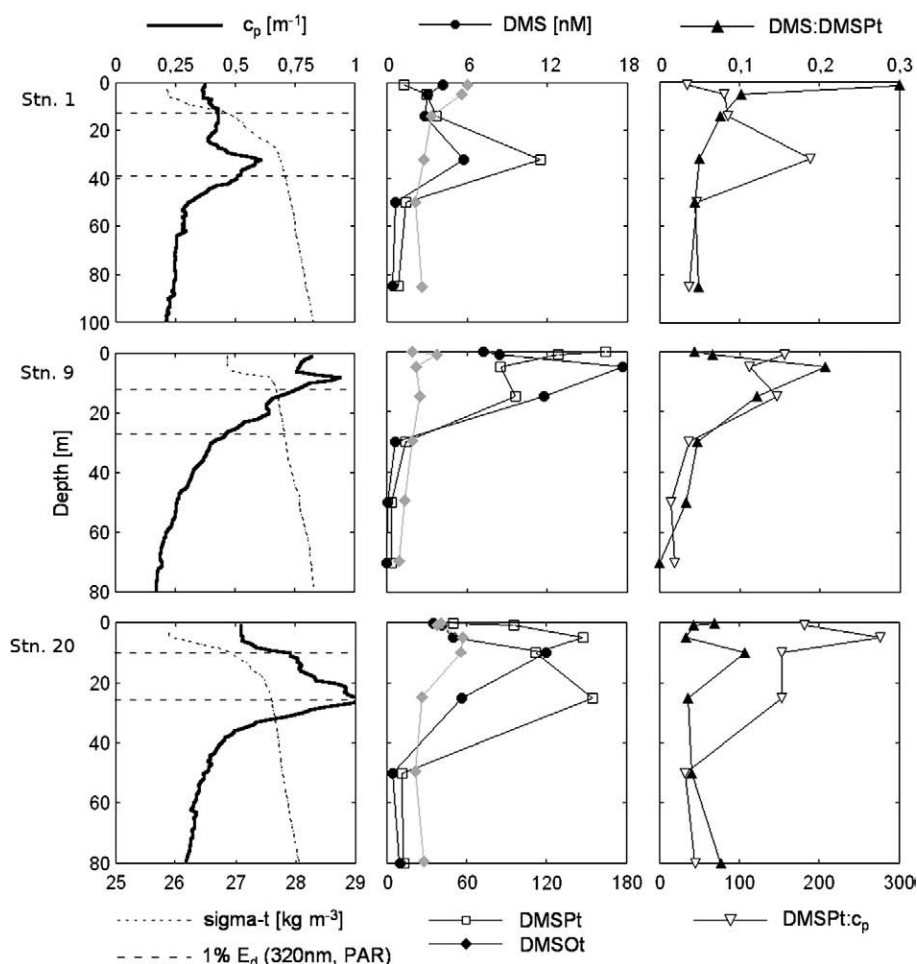
Fig. 2. Vertical profiles at Stn. 1 (PSW, EGC; top panels), 9 and 20 (AW, Fram Strait area; middle and bottom panels) showing distinct biomass and dimethylated sulfur distributions with depth. These stations are suggested to represent different stages of the bloom: early (9) middle (20) and late (1).

euphotic zone) DMSPt was 65.5 ± 50 nM (average ± SD), with a maximum of 163 nM, and below that depth it was never above 15 nM. DMS concentrations had a vertical pattern different from that of its precursor compound. It generally decreased from the subsurface to the deepest waters analyzed (85 m), although at some stations a second DMS peak was found at the depth of the c_p maximum. In the euphotic zone, DMS was typically around 5.3 ± 4 nM, reaching up to 18.3 nM. Below 40 m depth, DMS concentrations rarely exceeded 1 nM. Despite varying in a narrower range than the preceding compounds, DMSOt also exhibited a clear vertical pattern, with a mean of 51 ± 13.6 nM in surface waters and down to 5 m depth, and 27 ± 10.5 nM below that depth. DMSOd accounted for $58 \pm 8\%$ of DMSOt in surface waters where it was measured ($n = 9$, data not shown). In the context of *Phaeocystis* blooms, the DMSPt and DMS concentrations we report fall in the mid-low range (Stefels et al., 2007). To our knowledge, no review exists on DMSO pools and dynamics during *Phaeocystis* blooms. Integrating vertically the concentrations in the euphotic zone, we obtain that DMSPt, DMSOt and DMS accounted for $67 \pm 5\%$, $28 \pm 5\%$ and $5 \pm 2\%$ of the total dimethylated sulfur, respectively. Due to shallow mixing, only a minor fraction of the sulfur pools was in the UML: approximately 20% of DMS and DMSOt, and only 10% of DMSPt.

3.2.2. Surface concentrations and sea ice

The highest spatial variability for the three sulfur compounds was encountered in subsurface waters (0.1 and 1 m depth, Fig. 3). DMS concentrations spanned one order of magnitude (1.5 to 18.3 nM), and were slightly lower at 0.1 m (mean 5.3 nM) compared to 1 m (mean 6.3 nM). DMSPt concentrations had an even broader span (5.6 to

163.6 nM), but were not different at 1 m or 0.1 m (overall mean around 70 nM). DMSOt concentrations varied between 19 and 85 nM, with a mean of 51 nM and slightly more disperse values at 0.1 m. Consistent with the differences found in surface biomass between station types, surface DMSPt was clearly higher at AW stations (102.5 ± 31.3 nM) than those at PSW and PSWi (18.8 ± 6.8 nM). However, no significant differences were found for DMS and DMSOt between station types (Fig. 3).

DMSOt (range of 7.9–12.2 nM) but no DMSPt were found in snow and surface ice, which supports an atmospheric origin of DMSO (Andreae, 1980). At two stations, higher amounts of DMSPt and DMSOt were found in bottom ice, with maximum concentrations of 90 and 24 nM respectively. In this case, a biological origin was feasible, but the concentrations were very low compared to the µM levels reported by Levasseur et al. (1994), or the hundred nM levels reported by Bouillon et al. (2002). Our results indicate that sea ice was not a major source of dimethylated sulfur in the region at that time of the year, and therefore they will not be discussed.

3.3. Biological turnover of DMS

3.3.1. Production and consumption rates

DMDS amended incubations in all cases caused accumulation of DMS over that in non-amended incubations (Fig. 4). Gross DMS production rates at the surface (1 m) ranged between 1.4 nM d^{-1} (Stn. 1) and 14.8 nM d^{-1} (Stn. 42, Table 2). The stations belonging to the PSW group (EGC) showed the lowest gross production rates (<1.5 nM d^{-1}), while in strongly blooming waters and in the vicinity of the ice (AW and PSWi) gross production rates were higher (mean of 6.4 nM d^{-1}). At the
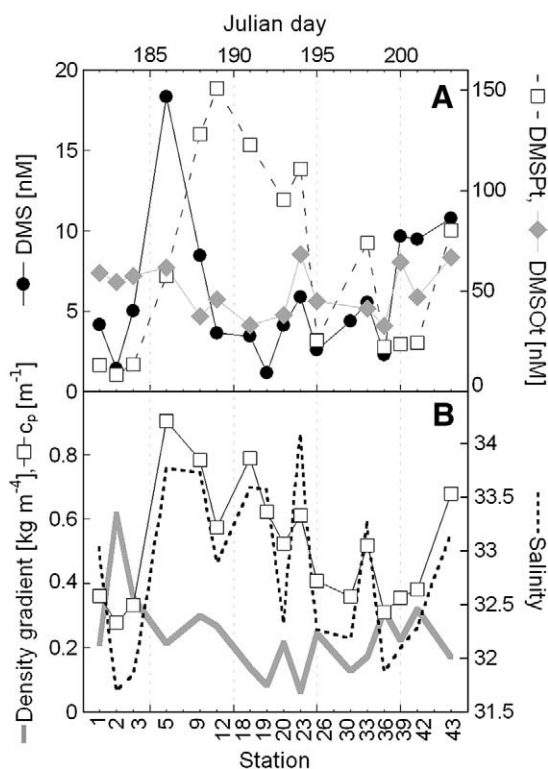
Fig. 3. Surface water properties at all 17 stations and day of sampling (July 2007): A) concentration of dimethylated sulfur compounds; and B) ice-induced stratification, salinity and planktonic microbial biomass. All values correspond to 1 m depth except the sigma-t gradient (depth of the maximum gradient at the pycnocline).

fluorescence maximum, gross DMS production was also lowest at PSW stations (<1 nM d^{-1}) with an absolute minimum at Stn. 3 (0.4 nM d^{-1}). The maximum was found at Stn. 12, with 12.7 nM d^{-1}. Bacterial DMS consumption at the surface had its minimum at Stn. 26 (0.37 nM d^{-1}) and its maximum at Stn. 42 (12.9 nM d^{-1}). At the fluorescence maximum, DMS consumption ranged between 0.8 nM d^{-1} (Stn. 3) and 16.8 nM d^{-1} (Stn. 20). No clear differences were found in DMS consumption between water masses and/or ice influence at either depth. The overall mean of bacterial DMS consumption in surface waters was 4.3 nM d^{-1}, slightly below the mean gross production of 5.5 nM d^{-1} (Table 2). At the fluorescence maximum, conversely, DMS consumption was 7.4 nM d^{-1}, slightly above the mean gross production of 5.9 nM d^{-1}.
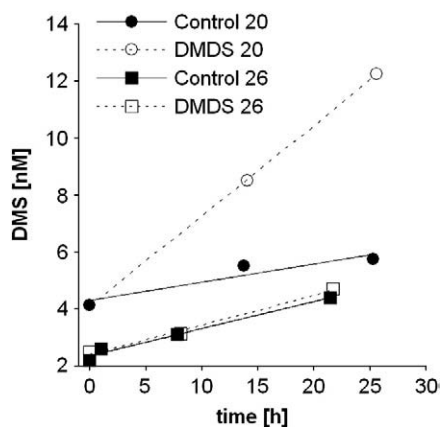
Fig. 4. Examples of DMS evolution during biological process incubations at Stns. 20 and 26 (1 m depth).

3.3.2. Consumption and production rate constants

The rate constants (K) of the biological process incubations were calculated as the process rate (nM d^{-1}) divided by the initial DMS concentration (nM). The Ks of gross DMS production (K_{gp}) in both surface and fluorescence maximum samples lay between 0.30 d^{-1} (Stn. 3) and 2.2 d^{-1} (Stn. 19 surface and Stn. 12 fluorescence maximum, Table 2). DMS consumption rate constants (K_{bc}) were in the same range, from 0.14 d^{-1} (Stn. 26 surface) to 2.2 d^{-1} (Stn. 19 surface). The mean rate constants in surface samples were 1.2 d^{-1} for production and 0.9 d^{-1} for bacterial consumption, while at the fluorescence maximum the mean Ks were 1.3 and 1.7 d^{-1} for production and consumption respectively (Table 2).

3.3.3. Dark versus light incubation

At Stn. 42, dark and light incubations were performed with the same surface water sample, to investigate whether solar radiation affected biological production and consumption. Duplicate bottles were incubated with the following treatments: DMDS-light, control-light and control-dark. In incubations kept under the sunlight, DMS evolution was corrected using the photochemical rate constant obtained from parallel photochemistry incubations. Net biological DMS production in the light (1.9 nM d^{-1}) was clearly higher than in the dark (-2.3 nM d^{-1}), but the lack of dark DMDS incubations obscures the interpretation of these results (see *Discussion*).

3.4. DMS photolysis

The rate constants of DMS photolysis in photochemistry experiments ranged from 0.50 d^{-1} (Stn. 42) to 1.14 d^{-1} (Stn. 20), with a mean of 0.81 d^{-1}. Once extrapolated to the whole UML, the photolysis rate constant ($K_{photo,UML}$) was on average 0.72 d^{-1}, equivalent to a mean in situ photolysis rate of 3 nM d^{-1} (Table 3).

3.5. Sea–air DMS flux

3.5.1. Sea surface fluxes

DMS emission fluxes at the sea surface varied between 0.5 µmol m^{-2} d^{-1} (Stn. 19) and 22.5 µmol m^{-2} d^{-1} (Stn. 42), with a mean flux of 6.5 µmol m^{-2} d^{-1}. Volumetric ventilation rates in the ML ranged from 0.07 nM d^{-1} (Stn. 19) to 2.77 nM d^{-1} (Stn. 36), averaging 1.12 nM d^{-1}. The corresponding range of ventilation rate constants ($K_{vent,UML}$) was 0.056–0.69 d^{-1} (mean 0.23 d^{-1}).

4. Discussion

4.1. Factors controlling dimethylated sulfur compound concentrations

4.1.1. Vertical profiles

The statistical analysis of dimethylated sulfur compounds concentration together with CTD variables revealed a different pattern for each of the compounds (Table 4). DMSPt was strongly correlated to indicators of algal biomass (especially to c_p) and negatively correlated with depth. The stepwise regression indicated that c_p was the only predictor worth including in the regression model, that is, with a slope significantly different from zero at the 0.05 level ($r^2 = 0.67$, $p < 10^{-7}$). Forcing the addition of the next "most significant" term in the model (fluorescence) increased the variance explained only to 70% ($r^2 = 0.70$). The high predictability of DMSPt from c_p probably stemmed from the abundance of *P. pouchetii* during our study.

Intracellular DMSP concentrations in *Phaeocystis* are roughly 10 to 100 times higher than in diatoms, and in the same order of magnitude than in dinoflagellates (Hatton and Wilson, 2007; Stefels et al., 2007). The dominance of *Phaeocystis* and the elevated DMSPt:Chl *a* during our cruise (38.6 nmol/µg), a value in the upper edge of those found in *Phaeocystis* blooms (Stefels et al., 2007), suggests that *Phaeocystis* was the dominant species in terms of its contribution to the DMSPt pool.

Table 2
Gross DMS production (GP) and biological DMS consumption (BC) rates for the UML (1 m) and fluorescence maximum samples, with the corresponding rate constants (K_{gp} and K_{bc}). The standard error of the slope (or the propagated SE when required) is shown in parentheses.

Station	Sample depth (m)	GP rate (nM d^{-1})		BC rate (nM d^{-1})		K_{gp} (d^{-1})		K_{bc} (d^{-1})	
UML (1 m depth)									
1		1.4	(0.89)	2.9	(1.5)	0.32	(0.21)	0.70	(0.37)
3		1.5	(0.74)	1.3	(0.77)	0.30	(0.15)	0.26	(0.15)
9		6.8	(0.60)	6.6	(0.87)	0.80	(0.07)	0.78	(0.10)
12		6.9	(0.16)	1.6	(0.43)	1.9	(0.04)	0.45	(0.12)
19		2.6	(0.19)	2.5	(0.19)	2.2	(0.16)	2.2	(0.17)
20		7.6	(0.12)	6.1	(0.56)	1.8	(0.03)	1.5	(0.14)
26		2.5	(0.22)	0.4	(0.31)	0.95	(0.08)	0.14	(0.12)
42		ND		17.1[a]	(0.91)	ND		1.8[a]	(0.10)
42 light		14.8	(0.50)	12.9	(0.84)	1.6	(0.05)	1.4	(0.09)
Mean		**5.5**		**4.3**		**1.2**		**0.9**	
Fluorescence maximum									
1	34	0.62	(1.18)	3.90	(1.92)	0.3	(0.57)	1.9	(0.93)
3	25	0.41	(0.36)	0.82	(0.46)	0.27	(0.24)	0.54	(0.31)
9	15	5.2	(0.67)	5.1	(1.6)	1.8	(0.23)	1.7	(0.57)
12	9	12.7	(2.7)	16.8	(2.8)	2.3	(0.48)	3.0	(0.50)
20	25	10.6	(1.1)	10.4	(1.3)	1.7	(0.18)	1.6	(0.20)
Mean		**5.9**		**7.4**		**1.3**		**1.7**	

[a] Determined from GP in the light and BC in the dark. Not included in the means.

Assuming that almost all DMSP was particulate (after Kiene and Slezak, 2006), the DMSPt:c_p ratio can be taken as a biomass-specific DMSP concentration, that is, a proxy for intracellular DMSP concentration. Even more, the evidence of low feeding rates on *Phaeocystis* by zooplankton, supported by field data from our cruise (Calbet et al., submitted for publication) and reported in the literature (review by Nejstgaard et al., 2007), suggests that most DMSP was algae-bound. In Fig. 2 it can be observed that the DMSPt:c_p ratio had a vertical pattern somewhat different from that of DMSPt alone. Whether this distinct pattern resulted from differences in community composition or in physiological status with depth (and bloom phase) remains an open question.

In the case of DMS, only correlations with c_p and DMSPt (positive) and depth (negative) were significant individually. DMSPt was the only predictor accepted in the stepwise regression model ($r^2 = 0.42$, $p < 10^{-4}$), and forcing the addition of depth in the predictor matrix (the second most significant term) increased the explained variance only to 46%. Not surprisingly, DMS was less predictable than its precursor DMSP, due to the greater weight of physical forcing on its cycling (Simó and Pedrós-Alió, 1999). DMS concentrations and, most important, the DMS:DMSPt ratio, were highest in surface waters (Fig. 2). This might indicate that, despite greater rates of DMS photooxidation and ventilation close to the surface, an elevated exposure to solar irradiance favored a more efficient conversion of DMSP to DMS by the microbial food web.

Compared to the other sulfur species, DMSOt concentrations were strongly related to abiotic parameters such as density (or salinity) and depth, and increased clearly towards the surface. Interestingly, water density (sigma-t) was the only predictor admitted in the stepwise regression model ($r^2 = 0.49$, $p < 10^{-3}$). This means that this parameter did the best at summarizing the environmental conditions that led to DMSOt accumulation. Production of dissolved and particulate DMSO through light-mediated biotic and abiotic processes is relatively well documented. Those processes include (a) DMSO production due to DMS photochemistry (Hatton, 2002; Kieber et al., 1996) and algal DMSP and DMS oxidation (del Valle et al., 2007b; Hatton and Wilson, 2007; Simó et al., 1998; Sunda et al., 2002), and (b) bacterial DMS oxidation, with a tendency towards higher DMSOd yields in the UML, (where lower bacterial DMS consumption rates normally occur), and higher DMS carbon utilization and sulfate production in deeper waters (del Valle et al., 2007a, 2009). In the stably stratified surface waters of the Arctic, lower water density implies a higher exposure to solar radiation in the mid or long term. In fact, a correlation existed between the strength of the stratification and DMSOt concentrations. Finally, DMSOt concentrations could be interpreted in terms of bloom phase, with higher values being associated with late bloom stages: at Stn. 9, where a situation of early bloom was found, DMSOt concentrations integrated over the top 100 m were 40% lower than at Stn. 1 or 20.

4.1.2. Surface concentrations

The amount of DMSPt, DMS and DMSOt at the immediate subsurface (0.1 m) compared to 1 m depth was very similar, with a ratio that approached 1, on average, for all three compounds. The existing variability, however, can tell us about the factors controlling each of the sulfur species. An overall higher variability was found for DMS (34% of the range about the mean) than for DMSPt (24%) or DMSOt (23%).

When we plotted DMSPt concentrations together with physical variables and biomass data at the surface, a clear picture of the factors explaining its surface distribution emerged (Fig. 3). Salinity and temperature at 1 m depth were positively correlated (Spearman's

Table 3
Integrated irradiance during deck board incubations, CDOM characteristics (absorption coefficient at 300 nm and spectral slope in the 300–400 nm range), and K_{photo} obtained from the experiments and calculated for the entire UML. The sky was clear at Stns. 20 and 26 and heavily overcast at Stns. 39 and 42. Incubations generally started at 14:00 and ended between 21:00 and 02:00.

Station	Experiment							UML		
	UVB (kJ m^{-2})	UVA (kJ m^{-2})	PAR (mol photons m^{-2})	$a_{CDOM,300}$ (m^{-2})	$S_{300-400}$ (nm^{-1})	K_{photo} (d^{-1})	K_{photo}/UVR (m^2 kJ^{-1} d^{-1})	$K_{d,340}$ (m^{-1})	$K_{photo,UML}$ (d^{-1})	Photo rate (nM d^{-1})
20	5.0	160	6.9	0.94	0.010	1.14	0.007	0.40	1.05	4.43
26	5.6	200	8.7	0.38	0.023	0.69	0.003	0.44	1.04	2.6
39	1.8	59	2.3	0.43	0.026	0.93	0.015	0.35	0.55	3.01
42	2.6	85	3.2	0.58	0.014	0.5	0.006	0.29	0.23	1.85

Table 4
Correlation table for oceanographic variables and sulfur compounds in vertical profiles. The values are Pearson correlations, and are marked in bold when significant (p<0.01). The maximum number of X–Y pairs available has been used in each variables combination. N is 61, 54 and 51 for DMS, DMSPt and DMSOd respectively.

	DMSOt	DMS	DMSPt
Depth	**− 0.65**	**− 0.47**	**− 0.40**
Temperature	− 0.25	0.19	0.24
Salinity	**− 0.71**	− 0.14	− 0.04
Sigma-t	**− 0.76**	− 0.23	− 0.13
Sigma-t gradient	**0.48**	0.04	0.02
O_2	− 0.25	− 0.09	− 0.01
c_p	0.09	**0.52**	**0.81**
Fluorescence	− 0.33	0.16	**0.50**
DMSPt	0.07	**0.47**	
DMS	0.27		

r = 0.68, p < 10^{-3}) illustrating the effect of ice melting. In turn, both variables were negatively correlated with the density gradient at the base of the mixed layer (r = −0.77, p < 10^{-4}, and r = −0.5, p < 0.05, for salinity and temperature, respectively), which means that ice melting controlled the strength of surface stratification. In addition, plankton biomass (c_p) varied inversely with salinity (r = −0.87, p < 10^{-6}) and the density gradient (r = −0.47, p < 0.05). This illustrates that recent meltwaters were not a good growth medium for DMSP producers (*Phaeocystis*), an inference supported by measurements of primary production and phytoplankton cells viability done in the same cruise (Duarte et al., in preparation; Lasternas and Agustí, in revision). Indeed, surface DMSPt and c_p were highly correlated (r = 0.87, p < 10^{-4}). The higher concentrations of algal biomass and DMSPt in less isolated surface waters suggest that the DMSP stock at the surface was fed by living cells and detrital algal material entrained from waters below.

In the case of DMS, the picture was somewhat different. It seemed to follow DMSPt and biomass concentrations at some stations, while at others much of the DMS expected from its precursor had vanished. Indirect evidence that solar radiation was the main factor accounting for the "missing" DMS at those stations is provided in Fig. 5. If we examine the relationship between the DMS:DMSPt ratio and the mean solar irradiance during the 24 h previous to sampling, a significant negative correlation exists (r = −0.82, p < 10^{-3}). Further evidence is found in the fine-scale DMS vertical gradient (previously normalized to the mean surface DMS concentration to account for the more pronounced gradients found at high-DMS stations), which also appears related to the previous surface irradiance (r = −0.73, p < 0.01, after removing one outlier). Generally the DMS concentrations increased towards the surface when the daily mean irradiance was below 200 W m^{-2}. Conversely, if the daily mean irradiance was greater, then the DMS concentrations decreased towards the surface, indicating that DMS photolysis was able to counteract biological DMS production. Finally, lower UML-averaged DMS concentrations were associated with higher UML-averaged irradiances (r = −0.60, p < 0.05). Adding wind speed did not help explain more of the variance of the DMS variables, indirectly indicating an overall minor impact of sea–air flux in DMS cycling compared to solar radiation.

Surface DMSOt displayed less variability across stations than its precursor compounds (Fig. 3). It was correlated to DMS (r = 0.58, p < 0.05) but not to DMSPt (r = −0.22, p > 0.05) or c_p (r = 0.02, p > 0.05). This points to DMS photochemistry and bacterial DMS consumption as the main sources of DMSO(d), with algal production playing a secondary role. With a mean UML DMS of 5.5 nM, a mean $K_{photo,UML}$ of 0.7 d^{-1} with a DMSOd yield of 50%, and a mean K_{bc} of 0.9 d^{-1} with a DMSOd yield of 20% (yields taken from del Valle et al., 2009), the DMSOd produced daily by DMS photochemistry (2 nM d^{-1}) would be twice that produced by microbial DMS oxidation. This would imply a turnover time of 10 d for the mean surface DMSOd of 30 nM in our study area. These figures are in quite good agreement with those presented in del Valle et al. (2009) for the

Ross Sea. Particularly, the calculated DMSOd turnover time falls between those found for the early and late phase of the *Phaeocystis antarctica* bloom in that work. Surprisingly, we found a negative correlation between DMSOt and the UML-integrated irradiance (r = -0.67, p < 0.01). This seems to contradict the statements made above, but could also indicate a solar radiation induced removal of DMSO. Our knowledge of DMSO removal pathways in oceanic waters is too poor to make better inferences.

4.2. Factors controlling biological DMS cycling

Biological DMS cycling was very fast, with turnover times as short as half a day encountered both in the UML and in the fluorescence maximum. On average, biological turnover occurred in 2.2 d and was never longer than 4 d (except at Stn. 26, where an extremely low bacterial consumption rate was observed). This range is very similar to that found by Wolfe et al. (1999) in the Labrador Sea. In the following paragraphs we will examine what factors controlled the rates and rate constants (Ks) of biological DMS cycling, with emphasis on those taking place in the UML.

DMSP cleavage in our study area was probably dominated by algal lyases. *Phaeocystis* species have been shown to dominate DMSP lyase activity in blooms where they occur in large numbers (Stefels et al., 1995). In the Labrador sea, Cantin et al. (1999) found that most DMSP lyase activity was found in the 2 – 11 and >20 μm size fractions, although they could not refute that part of the DMSP lyase activity was due to attached bacteria. We could not quantify how much of the
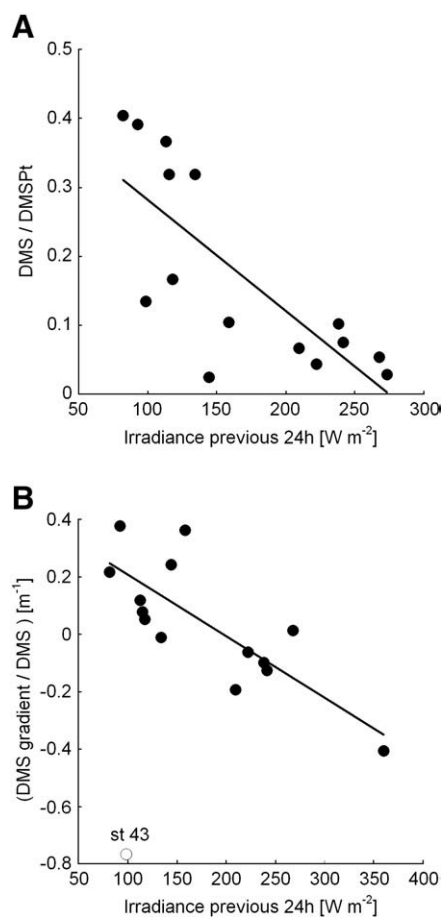
Fig. 5. Indirect evidence of the impact of photochemistry on surface DMS concentrations: relationship between the mean surface irradiance during the previous day and A) the ratio DMS:DMSPt at 1 m depth; and B) the gradient of DMS concentration in the first meters of the water column.
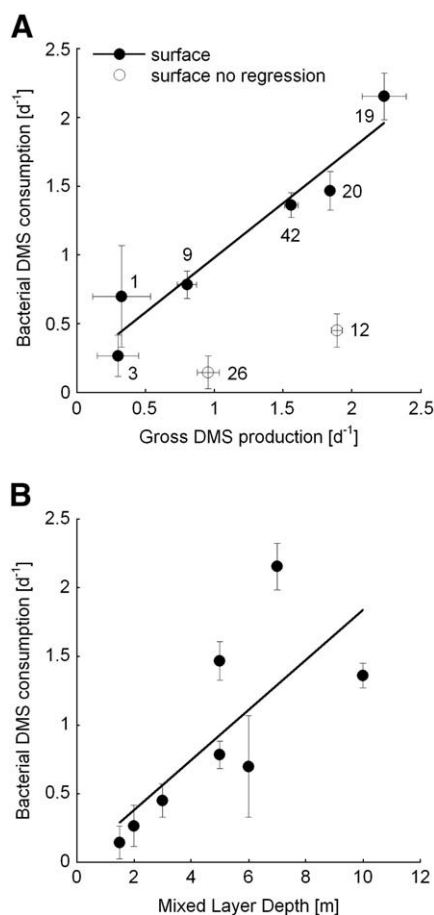
Fig. 6. Factors controlling bacterial DMS consumption in the UML: A) relationship between DMS production and consumption (1 m depth samples). Only points represented by the filled squares are used in the linear least squares fit, which has a slope of 0.79 ± 0.3. The station number is indicated adjacent to each point; and B) relationship between DMS consumption and the MLD.

gross DMS production was grazing-mediated, but a low impact of micro- and mesozooplankton grazing on algal biomass was inferred from dilution experiments (Calbet et al., submitted for publication). This suggests that much of the DMSP might be directly cleaved after lysis of damaged cells, or upon DMSP exudation, which occurs at high rates in *Phaeocystis* compared to other phytoplankton (Laroche et al., 1999). In any case, most DMSP cleavage would be done by either membrane-bound enzymes of healthy algal cells (Stefels and Dijkhuizen, 1996) or by free (dissolved) lyases from lysed cells. The good correlation between gross community DMS production rates and in situ DMSPt concentrations ($r = 0.75$, $p < 0.01$, Stn. 42 excluded) supports this suggestion.

The above correlation includes data from both the surface (UML) and the fluorescence maximum, which did not seem to behave differently in terms of gross DMS production. The exception was Stn. 42 (surface), where a DMS production rate disproportionately high for the in situ DMSPt concentration was obtained. The ratio of gross DMS production (GP) to the DMSPt stock gives an estimate of the DMSPt fraction that was transformed daily by the cleavage pathway. GP/DMSPt was between 0.01 and 0.16 d^{-1} at all stations, except at Stn. 42 (0.54 d^{-1}), where incubations were done in the light. Enhancement of DMS production as a result of high light or UV stress has been previously suggested by experimental results (Hefu and Kirst, 1997; Stefels, 2000; Sunda et al., 2002), and by model simulations (Toole et al., 2008; Vallina et al., 2008). Such stimulation by sunlight would have a strong impact on DMS budgets, but still awaits a clear experimental confirmation.

Pooling together surface and fluorescence maximum incubations, gross DMS production and bacterial consumption rates appeared tightly coupled at most stations ($r = 0.76$, $p < 001$). From a temporal point of view, the rise in DMS production and, therefore, in DMS concentrations, would trigger the response of DMS consumers. DMS consumption rates did not seem to saturate at the highest DMS concentrations observed, and represented around 100% or more of the DMS produced in the fluorescence maximum (Table 2), and 80% in the UML (Fig. 6A). This coupling is a common feature of DMS cycling (see review by Simó, 2004) and has been observed in diverse systems and with varied methodological approaches. Looking at surface rates, however, we can see that some stations deviated from the general coupling pattern (Stn. 12 and 26; Fig. 6A). To explore which factors could explain this decoupling, a correlation table was calculated including K_{gp}, K_{bc}, and environmental variables (Table 5). Among the factors considered, we found a strikingly good correlation between K_{bc} and MLD ($r = 0.81$, $p < 0.05$, Fig. 6B). Considering that the MLD regulates the exposure of plankton to solar radiation, we hypothesize that bacterial DMS consumers were inhibited by sunlight at the stations with the shallowest MLD (Stn. 3, 12 and 26), thus decoupling DMS consumption rates from gross production rates. This agrees with previous works reporting severe photoinhibition of DMS consumption in different oceanic regions (Toole et al., 2006). However, if that was the case, why was K_{bc} not strongly correlated ($r = -0.11$, $p > 0.10$) to the previous 24 h solar exposure?

A possible response lies in the timespan used to calculate the UML-integrated irradiance, that is, how long we go back in time to define the radiative history of the microbial community. Taking into account that our incubations were conducted in the dark, and that bacterial recovery from photodamage can take place over hourly time scales (Kaiser and Herndl, 1997), the observed effects should have occurred through succession in the bacterioplankton community. Selection of photoresistant bacteria would operate in a time scale of days by reducing the numbers of the less photoresistant bacterial populations, eventually affecting the DMS consumers. However, limited knowledge on the taxonomy of DMS consumers (Vila-Costa et al., 2006a; Schäfer, 2007) hampers our understanding of their response to solar radiation. Alternatively, slow or lack of dark recovery in the biochemical machinery implicated in DMS metabolism could also cause the observed effect.

4.3. Links between ice-induced stratification and sulfur cycling

4.3.1. Short term DMS budgets and sea-air flux

DMS cycling is characterized by its fast turnover. Adding up the three main processes that remove DMS from the UML in stratified conditions (that is, bacterial consumption, photolysis and degassing to the atmosphere) a mean turnover time of 0.8 d was obtained for our cruise. Based on measured K_{bc}, $K_{photo,UML}$ and $K_{vent,UML}$, we calculated that the mean relative contribution to DMS removal by bacterial

Table 5

Factors potentially controlling DMS production and removal in the UML. The values are Spearman correlations, and the asterisks denote significance at the $p < 0.05$(**) or $p < 0.10$ (*) level.

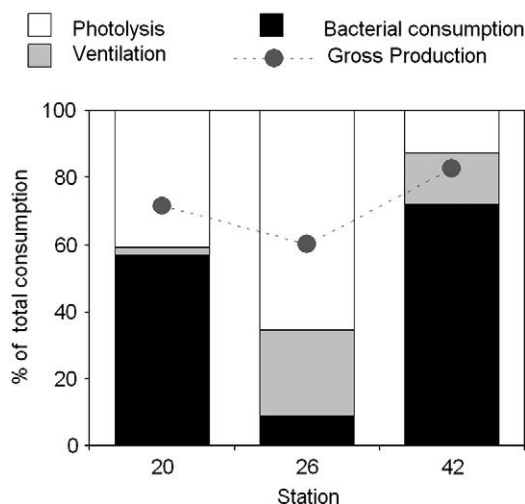|	K_{gp}	K_{bc}
Temperature	−0.67*	−0.38
Salinity	0.40	0.40
MLD	0.32	0.81**
Sigma-t gradient pycnocline	−0.48	−0.43
Irradiance previous 24 h	0.04	−0.11
DMS	−0.40	0.02
DMSPt	0.75*	0.21
c_p	0.62	0.45
Bacterial production nn1 m)	−0.13	−0.05
K_{gp}		0.57

Fig. 7. Relative contribution of DMS loss processes to its removal from the UML, and comparison with the relative gross DMS production.

consumption, photolysis and ventilation was 46%, 40% and 14% respectively. Fig. 7 shows that a shallower MLD (Stn. 26) caused simultaneously an increase in $K_{photo,UML}$ as a consequence of enhanced solar radiation doses, an increase of $K_{vent,UML}$ through the reduction of the volume of water exposed to wind stress, and a reduction of K_{bc} probably due to photoinhibition.

Another relevant information contained in Fig. 7 is that measured rates of gross DMS production were only able to supply 60 – 80% of the total DMS consumed. In our opinion, this imbalance suggests that gross DMS production was underestimated by dark DMDS amended incubations, a fact that was also suggested by the distinct behavior of

the only light incubation performed (Stn. 42), as described above. Few works exist that report oceanic DMS budgets based on actual measurements of each of the processes involved, since normally one of them is calculated by budgeting upon assumption of steady state, a condition that approximately holds over a daily time scale. Due to methodological difficulties, gross DMS production is most frequently the indirectly calculated flux (e.g., Bailey et al., 2008). All in all, comprehensiveness makes our data more valuable, despite methodological shortcomings related to dark incubations and the inhibitor method.

Focusing now on the sea-air DMS flux, we see that the mean value in our cruise (6.5 μmol m^{-2} d^{-1}) is above that reported for a cruise conducted in 1991 in a nearby region (2 μmol m^{-2} d^{-1}; Leck and Persson, 1996). The same authors report DMS concentrations to decline, from a maximum of ca. 10 nM in early August, at a rate of 30% per week in the Arctic ice-margin region through August and September. Thus, our cruise probably took place during the time of the year when highest DMS emissions occur in the Fram Strait area. This timing of DMS emissions is different from that reported for the Barents sea, where the peak occurs earlier in the season because of earlier sea ice retreat (Matrai and Vernet, 1997; Gabric et al., 1999). However, the biogeochemical settings reported and simulated (respectively) in those studies differ significantly from ours, in that they found deeper mixing conditions and light limited phytoplankton growth.

Examining our flux calculations, it can be observed that seawater DMS concentrations and wind speed contributed almost equally to determine the DMS flux. But, did wind speed exert a more indirect influence on DMS cycling? With the help of stepwise linear regression, we found that wind speed alone (over the previous 24 h) explained 52% of the variance of the MLD ($p<0.01$, $n=16$). Adding to the model the strength of stratification at the base of the UML, the variance of the MLD explained increased to 71% ($p<10^{-3}$, $n=16$), indicating that
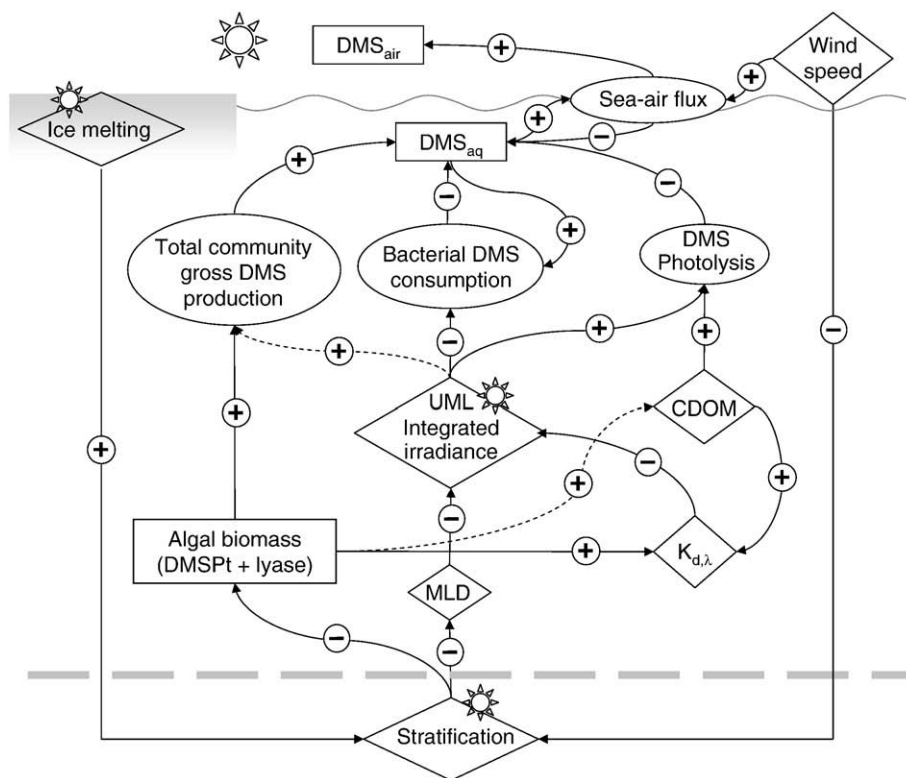

Fig. 8. Proposed conceptual scheme linking dimethylated sulfur dynamics with surface stratification and ice melt dynamics during the *Phaeocystis* bloom. Rectangles: chemical and biological stocks and concentrations (measured, except DMS$_{air}$); diamonds: physical and chemical environmental forcings; ellipses: measured DMS fluxes (rates); round labels: sign of the interaction in the direction of the arrow; continuous lines represent connections that can be deduced from the data presented, or that were already well established; dashed lines represent proposed connections.

meltwater indeed helped maintain the strong and shallow stratification conditions. In the paragraphs and sections above, we have emphasized the control exerted by the pycnocline in the supply of cells and detritus from the richer waters underneath, and the importance of the mixing depth for the balance between competing DMS sinks. Since sea-air flux was generally a minor sink for DMS in the UML, it might well be that wind exerted the greatest influence on DMS cycling through partially controlling mixing depths, rather than through direct DMS emission.

The discussion hitherto has addressed the factors that seemed to modulate DMS cycling processes in the short term according to observations. Our data capture a snapshot of the DMS cycle in the Arctic ice edge in the ice melt season, as summarized in Fig. 8.

4.3.2. Mid and long term

Short term DMS dynamics in any marine environment take place within a physico-chemical setting that influences cycling processes both directly and by driving plankton community composition and succession. In our study case, physical climatic forcing (ocean circulation, ice melting) drove water productivity and exposure to solar radiation, two factors with major influence in DMS cycling. A third factor with a particularly large importance was the presence of *P. pouchetii*. The success of this species may be due to a number of features. Among them, its ability to avoid grazers through colony formation, and its ability to thrive in shallow-mixed, ice-stratified, and highly irradiated waters seem key properties (Schoemann et al., 2005). Our observation of marked absorption peaks around 330 nm in CDOM spectra, which probably indicates leakage of mycosporine-like aminoacids from algal cells during GF/F filtration (Jeffrey et al., 1999) supports the importance of photoprotective mechanisms in ice-stratified waters. In addition, DMSP and its degradation compounds DMS and DMSO may constitute an important physiological adaptation to cope with radiative stress or nutrient demand-unbalanced growth (Stefels, 2000; Sunda et al., 2002). It turns out that any change in environmental conditions able to modify the strength, duration and extent of the ice edge *Phaeocystis* bloom, will have a strong impact on sulfur biogeochemistry in the Arctic, and on its role as an atmospheric DMS source.

During summer 2007, a historical minimum of Arctic sea ice was observed, together with an abnormal atmospheric circulation pattern and a deeper northwards penetration of Atlantic Waters. A sea ice-free Arctic summer is envisaged within the next few decades (Stroeve et al., 2008). Gabric et al. (2005) predicted a 90% increase in Arctic DMS emissions (in a scenario of atmospheric CO_2 tripling by 2080) as a result of a larger ice-free area and a longer growth season. This would represent a significant DMS-derived cooling effect. However, the numerical model used in that work appears too simple to capture the complex dynamics and spatial heterogeneity of the Arctic ecosystem. In summary, great changes in Arctic biogeochemistry (including volatile sulfur emissions) are likely to occur yet remain difficult to predict.

5. Conclusions

During July 2007, dimethylated sulfur dynamics in the Greenland Sea and Arctic Ocean were basically driven by phytoplankton biomass, i.e., the "bloom regime" postulated by Toole and Siegel (2004) as opposed to the (UV) stress regime found in oligotrophic regions. High potential for elevated summertime DMS concentrations and emissions did exist, owing to the dominance of *P. pouchetii*, but they were constrained by the fast photochemical and bacterial DMS consumption in the UML. Our findings portray a highly buffered system: vertical mixing causes alternation among DMS loss processes, preventing exaggerated consumption or build up.

Differences in DMS, DMSPt and DMSOt concentrations at the ocean surface resulted from the complex interaction of biological processes and physical (ultimately meteorological) forcing. Ice melting added complexity to the usual open-sea picture of DMS cycling, and created an isolated layer of fresher and colder water that acted as a highly irradiated trap for organisms and molecules, episodically entrained from below, and as a lid on the more productive waters underneath. This thin UML played a key role in regulating the flux of DMS to the atmosphere.

References

Andreae, M.O., 1980. Dimethylsulfoxide in marine and freshwaters. Limnol. Oceanogr. 25, 1054–1063.

Andreae, M.O., Crutzen, P.J., 1997. Atmospheric aerosols: biogeochemical sources and role in atmospheric chemistry. Science 276, 1052–1058.

Bailey, K.E., Toole, D.A., Blomquist, B., Najjar, R.G., Heubert, B., Kieber, D.J., et al., 2008. Dimethylsulfide production in Sargasso Sea Eddies. Deep Sea Res. II 55, 1491–1504.

Behrenfeld, M.J., Boss, E., 2003. The beam attenuation to chlorophyll ratio: an optical index of phytoplankton physiology in the surface ocean? Deep Sea Res. I 50, 1537–1549.

Bouillon, R.-C., Lee, P.A., de Mora, S.J., Levasseur, M., Lovejoy, C., 2002. Vernal distribution of dimethylsulphide, dimethylsulphoniopropionate, and dimethyl-sulphoxide in the North Water in 1998. Deep Sea Res. II 49, 5171–5189.

Brimblecombe, P., Shooter, D., 1986. Photo-oxidation of dimethylsulphide in aqueous solution. Mar. Chem. 19, 343–353.

Brugger, A., Slezak, D., Obernosterer, I., Herndl, G.J., 1998. Photolysis of dimethylsulfide in the northern Adriatic Sea: dependence on substrate concentration, irradiance and DOC concentration. Mar. Chem. 59, 321–331.

Calbet A, Saiz E, Almeda R, Movilla J, Alcaraz M, submitted for publication. Low microzooplankton grazing rates in the Arctic Ocean during a *Phaeocystis pouchetii* bloom (summer 2007): fact or artifact of the dilution technique? Submitted to Journal of Plankton Research.

Cantin, G., Levasseur, M., Schultes, S., Michaud, S., 1999. Dimethylsulfide (DMS) production by size-fractionated particles in the Labrador Sea. Aquat. Microb. Ecol. 19, 307–312.

Charlson, R.J., Lovelock, J.E., Andreae, M.O., Warren, S.G., 1987. Oceanic phytoplankton, atmospheric sulphur, cloud albedo and climate. Nature 326, 655–661.

Deal, C.J., Kieber, D.J., Toole, D.A., Stamnes, K., Jiang, S., Uzuka, N., 2005. Dimethylsulfide photolysis rates and apparent quantum yields in Bering Sea seawater. Cont. Shelf Res. 25, 1825–1835.

del Valle, D.A., Kieber, D.J., Kiene, R.P., 2007a. Depth dependent fate of biologically-consumed dimethylsulfide in the Sargasso Sea. Mar. Chem. 103, 197–208.

del Valle, D.A., Kieber, D.J., Bisgrove, J., Kiene, R.P., 2007b. Light-stimulated production of dissolved DMSO by a particle-associated process in the Ross Sea, Antarctica. Limnol. Oceanogr. 52, 2456–2466.

del Valle, D.A., Kieber, D.J., Toole, D.A., Bisgrove, J., Kiene, R.P., 2009. Dissolved DMSO production via biological and photochemical oxidation of dissolved DMS in the Ross Sea, Antarctica. Deep Sea Res. I 56, 166–177.

Duarte, C.M., Lasternas, S., Agustí, S., Regaudie-de-Gioux, A., Echeveste, P., Tovar-Sánchez, A., Arrieta, J.M., Álvarez, M., Dachs, J., Lacorte, S., Tauler, R., Galbán, C., Berrojálbiz, N., in preparation. Ice Melting Suppresses Primary Production in the Arctic Ocean.

Gabric, A., Matrai, P.A., Vernet, M., 1999. Modelling the production and cycling of DMSP and DMS during the vernal bloom in the Barents Sea. Tellus 51B, 919–937.

Gabric, A.J., Qu, B., Matrai, P., Hirst, A.C., 2005. The simulated response of dimethylsulfide production in the Arctic Ocean to global warming. Tellus 57B, 391–403.

Gasol, J.M., del Giorgio, P.A., Duarte, C.M., 1997. Biomass distribution in marine planktonic communities. Limnol. Oceanogr. 42, 1353–1363.

Hatton, 2002. Influence of photochemistry on the marine biogeochemical cycle of dimethylsulphide in the northern North Sea. Deep Sea Res. II 49, 3039–3052.

Hatton, A.D., Darroch, L., Malin, G., 2004. The role of dimethylsulphoxide in the marine biogeochemical cycle of dimethylsulphide. Oceanogr. Mar. Biol. 42, 29–56.

Hatton, A.D, Wilson, S.T., 2007. Particulate dimethylsulphoxide and dimethylsulpho-niopropionate in phytoplankton cultures and Scottish coastal waters. Aquat. Sci. 69, 330–340.

Hefu, Y., Kirst, G.O., 1997. Effect of UV- radiation on DMSP content and DMS formation of *Phaeocystis antarctica*. Polar Biol. 18, 402–409.

Howard, E.C., Henriksen, J.R., Buchan, A., Reisch, C.R., Bürgmann, H., Welsh, R., et al., 2006. Bacterial taxa that limit sulfur flux from the ocean. Science 314, 649–652.

IPCC, 2007. Climate change 2007: synthesis report. Contribution of Working Groups I, II and III to the Fourth Assessment Report of the Intergovernmental Panel on Climate Change [Core Writing Team, Pachauri, R.K and Reisinger, A. (eds.)]. IPCC, Geneva, Switzerland.

Jeffrey, S.W., MacTavish, H.S., Dunlap, W.C., Vesk, M., Groenewoud, K., 1999. Occurrence of UVA- and UVB-absorbing compounds in 152 species (206 strains) of marine microalgae. Mar. Ecol. Prog. Ser. 189, 35–51.

Johannessen, O.M., Bengtsson, L., Miles, M.W., Kuzmina, S.I., Semenov, V.A., Alekseev, G.V., et al., 2004. Arctic climate change: observed and modelled temperature and sea-ice variability. Tellus 56A, 328–341.

Kaiser, E., Herndl, G.J., 1997. Rapid recovery of marine bacterioplankton activity after inhibition by UV radiation in coastal waters. Appl. Environ. Microbiol. 63 (10), 4026–4031.

Keller, M.D., Bellows, W.K., Guillard, R.R.L., 1989. Dimethyl sulfide production in marine phytoplankton. In: Saltzman, E., Cooper, W.J. (Eds.), Biogenic Sulfur in the Environment. Am. Chemical Soc, pp. 167–182. New York.

Kieber, D.J., Jiao, J., Kiene, R.P., Bates, T.S., 1996. Impact of dimethylsulfide photochemistry on methyl sulfur cycling in the Equatorial Pacific Ocean. J. Geophys. Res. 101, 3715–3722.

Kiene, R.P., Linn, L.J., González, J.M., Moran, M.A., Bruton, J.A., 1999. Dimethylsulfonio-propionate and methanethiol are important precursors of methionine and protein–sulfur in marine bacterioplankton. Appl. Environ. Microbiol. 65, 4549–4558.

Kiene, R.P., Linn, L.J., Bruton, J.A., 2000. New and important roles for DMSP in marine microbial communities. J. Sea Res. 43, 209–224.

Kiene, R.P., Slezak, D., 2006. Low dissolved DMSP concentrations in seawater revealed by small volume gravity filtration and dialysis sampling. Limnol. Oceanogr.: Methods 4, 80–95.

Kirk, J.T.O., 1994. Light and Photosynthesis in Aquatic Ecosystems. Cambridge University Press, Cambridge. pp. 26–40.

Laroche, D., Vézina, A.F., Levasseur, M., Gosselin, M., Stefels, J., Keller, M.D., Matrai, P.A., Kwint, R.L.J., 1999. DMSP synthesis and exudation in phytoplankton: a modeling approach. Mar. Ecol. Prog. Ser. 180, 37–49.

Lasternas, S., Agustí, S., in revision. Phytoplankton community structure during the record Arctic ice-melting of summer 2007. Polar Biology.

Leck, C., Persson, C., 1996. The central Arctic Ocean as a source of dimethyl sulfide. Seasonal variability in relation to biological activity. Tellus 48B, 156–177.

Lee, P.A., de Mora, S.J., 1999. Intracellular dimethylsulfoxide (DMSO) in unicellular marine algae: speculations on its origin and possible biological role. J. Phycol. 35, 8–18.

Levasseur, M., Gosselin, M., Michaud, S., 1994. A new source of dimethyl sulfide for the Arctic atmosphere. Mar. Biol. 121, 381–387.

Lovelock, J.E., Maggs, R.J., Rasmussen, R.A., 1972. Atmospheric sulphur and the natural sulphur cycle. Nature 237, 452–453.

Malin, G., Kirst, G.O., 1997. Algal production of dimethyl sulfide and its atmospheric role. J. Phycol. 33, 889–896.

Matrai, P., Vernet, M., 1997. Dynamics of the vernal bloom in the marginal ice-zone of the Barents Sea: DMS and DMSP budgets. J. Geophys. Res. 102, 22965–22979.

Matrai, P.A., Vernet, M., Wassmann, P., 2007. Relating temporal and spatial patterns of DMSP in the Barents Sea to phytoplankton biomass and productivity. J. Mar. Syst. 67, 83–101.

Moritz, R.E., Bitz, C.M., Steig, E.J., 2002. Dynamics of recent climate change in the Arctic. Science 297, 1497–1502.

Nejstgaard, J.C., Tang, K.W., Steinke, M., Dutz, J., Koski, M., Antajan, E., Long, J.D., 2007. Zooplankton grazing on Phaeocystis: a quantitative review and future challenges. Biogeochemistry 83, 147–172.

Nightingale, P.D., Liss, P.S., Schlosser, P., 2000. Measurements of air–sea gas transfer during an open ocean algal bloom. Geophys. Res. Lett. 27, 2117–2120.

Oubelkheir, K., Claustre, H., Sciandra, A., Babin, M., 2005. Bio-optical and biogeochem-ical properties of different trophic regimes in oceanic waters. Limnol. Oceanogr. 50, 1795–1809.

Rudels, B., Björk, G., Nilsson, J., Winsor, P., Lake, I., Nohr, C., 2005. The interaction between waters from the Arctic Ocean and the Nordic Seas north of Fram Strait and along the East Greenland Current: Results from the Arctic Ocean-02 Oden expedition. J. Mar. Syst. 55, 1–30.

Sakshaug, E., 2004. Primary and secondary production in the Arctic Seas. In: Stein, R., Macdonald, R.W. (Eds.), The Organic Carbon Cycle in the Arctic Ocean, pp. 57–81.

Saltzman, E.S., King, D.B., Holmen, K., Leck, C., 1993. Experimental determination of the diffusion coefficient of dimethylsulfide in water. J. Geophys. Res. 98, 16481–16486.

Schäfer, H., 2007. Isolation of *Methylophaga* spp. from marine dimethylsulfide-degrading enrichment cultures and identification of polypeptides induced during growth on dimethylsulfide. Appl. Environ. Microbiol. 73, 2580–2591.

Schlitzer R, 2008. Ocean data view, http://odv.awi.de.

Schoemann, V., Becquevort, S., Stefels, J., Rousseau, V., Lancelot, C., 2005. Phaeocystis blooms in the global ocean and their controlling mechanisms: a review. J. Sea Res. 53, 43–66.

Simó, R., 2001. Production of atmospheric sulfur by oceanic plankton: biogeochemical, ecological and evolutionary links. Trends Ecol. Evol. 16, 287–294.

Simó, R., 2004. From cells to globe; approaching the dynamics of DMS(P) in the ocean at multiple scales. Can. J. Fish. Aquat. Sci. 61, 673–684.

Simó, R., Grimalt, J.O., Albaigés, J., 1996. Sequential method for the field determination of nanomolar concentrations of dimethyl sulfoxide in natural waters. Anal. Chem. 68, 1493–1498.

Simó, R., Hatton, A.D., Malin, G., Liss, P.S., 1998. Particulate dimethyl sulphoxide in seawater: production by microplankton. Mar. Ecol. Prog. Ser. 167, 291–296.

Simó, R., Pedrós-Alió, C., 1999. Short-term variability in the open ocean cycle of dimethylsulfide. Global Biogeochem. Cycles 13, 1173–1181.

Simó, R., Pedrós-Alió, C., Malin, G., Grimalt, J.O., 2000. Biological turnover of DMS, DMSP and DMSO in contrasting open-sea waters. Mar. Ecol. Prog. Ser. 167, 291–295.

Simó, R., Dachs, J., 2002. Global ocean emission of dimethylsulfide predicted from biogeophysical data. Global Biogeochem. Cycles 16, 1078. doi:10.1029/2001GB001829.

Simó, R., Archer, S.D., Pedrós-Alió, C., Gilpin, L., Stelfox-Widdicombe, C.E., 2002. Coupled dynamics of dimethylsulfoniopropionate and dimethylsulfide cycling and the microbial food web in surface waters of the North Atlantic. Limnol. Oceanogr. 47, 53–61.

Simó, R., Vila-Costa, M., 2006. Ubiquity of algal dimethylsulfoxide in the surface ocean: geographic and temporal distribution patterns. Mar. Chem. 100, 136–146.

Stefels, J., 2000. Physiological aspects of the production and conversion of DMSP in marine algae and higher plants. J. Sea Res. 43, 183–197.

Stefels, J., van Boekel, W.H.M., 1993. Production of DMS from dissolved DMSP in axenic cultures of the marine phytoplankton species *Phaeocystis* sp. Mar. Ecol. Prog. Ser. 97, 11–18.

Stefels, J., Dijkhuisen, L., 1996. Characteristics of DMSP-lyase in *Phaeocystis* sp. (Prymnesiophyceae). Mar. Ecol. Prog. Ser. 131, 307–313.

Stefels, J., Dijkhuizen, L., Gieskes, W.W.C., 1995. DMSP-lyase activity in a spring phytoplankton bloom off the Dutch coast, related to *Phaeocystis* sp. abundance. Mar. Ecol. Prog. Ser. 123, 235–243.

Stefels, J., Steinke, M., Turner, S., Malin, G., Belviso, S., 2007. Environmental constraints on the production and removal of the climatically active gas dimethylsulphide (DMS) and implications for ecosystem modelling. Biogeochemistry 83, 245–275.

Stroeve, J., Serreze, M., Drobot, S., Gearheard, S., Holland, M., Maslanik, J., Meier, W., Scambos, T., 2008. Arctic sea ice extent plummets in 2007. EOS Trans. Am. Geophys. Union 89, 2.

Sunda, W., Kieber, D.J., Kiene, R.P., Huntsman, S., 2002. An antioxidant function for DMSP and DMS in marine algae. Nature 418, 317–320.

Toole, D.A., Siegel, D.A., 2004. Light-driven cycling of dimethylsulfide (DMS) in the Sargasso Sea: closing the loop. Geophys. Res. Lett. 31, L09308. doi:10.1029/2004GL019581.

Toole, D.A., Slezak, D., Kiene, R.P., Kieber, D.J., Siegel, D.A., 2006. Effects of solar radiation on dimethylsulfide cycling in the western Atlantic Ocean. Deep Sea Res. I 53, 136–153.

Toole, D.A., Siegel, D.A., Doney, S.C., 2008. A light-driven, one-dimensional dimethyl-sulfide biogeochemical cycling model for the Sargasso Sea. J. Geophys. Res. 113, G02009. doi:10.1029/2007JG000426.

Vallina, S.M., Simó, R., 2007. Strong relationship between DMS and the solar radiation dose over the global surface ocean. Science 315, 506–508.

Vallina, S.M., Simó, R., Anderson, T.R., Gabric, A., Cropp, R., Pacheco, J.M., 2008. A dynamic model of oceanic sulfur (DMOS) applied to the Sargasso Sea: simulating the dimethylsulfide (DMS) summer paradox. J. Geophys. Res. 113, G01009. doi:10.1029/2007JG000415.

Vila-Costa, M., del Valle, D.A., González, J.M., Slezak, D., Kiene, R.P., Sánchez, O., Simó, R., 2006a. Phylogenetic identification and metabolism of marine dimethylsulfide-consuming bacteria. Environ. Microbiol. 8, 2189–2200.

Vila-Costa, M., Simó, R., Gasol, J.M., Harada, B., Slezak, D., Kiene, R.P., 2006b. Dimethylsulfoniopropionate (DMSP) uptake by marine phytoplankton. Science 314, 652–654.

Welsh, D.T., 2000. Ecological significance of compatible solute accumulation by micro-organisms: from single cells to global climate. FEMS Microbiol. Rev. 24, 263–290.

Wolfe, G.V., 2000. The chemical defense ecology of marine unicellular plankton: constraints, mechanisms, and impacts. Biol. Bull. 198, 225–244.

Wolfe, G.V., Kiene, R.P., 1993. Radioisotope and chemical inhibitor measurements of dimethyl sulfide consumption rates and kinetics in estuarine waters. Mar. Ecol. Prog. Ser. 99, 261–269.

Wolfe, G.V., Levasseur, M., Cantin, G., Michaud, S., 1999. Microbial consumption and production of dimethyl sulfide (DMS) in the Labrador Sea. Aquat. Microb. Ecol. 18, 197–205.

Yoch, D.C., Ansede, J.H., Rabinowitz, K.S., 1997. Evidence for intracellular and extracellular dimethylsulfoniopropionate (DMSP) lyases and DMSP uptake sites in two species of marine bacteria. Appl. Environ. Microbiol. 63, 3182–3188.

Zimmer-Faust, R.K., de Souza, M.P., Yoch, D.P., 1996. Bacterial chemotaxis and its potential role in marine dimethylsulfide production and biogeochemical sulfur cycling. Limnol. Oceanogr. 18, 1330–1334.